Journal of Applied Polymer Science

Fabrication of co-continuous poly(ε-caprolactone)/polyglycolide blend scaffolds for tissue engineering

Rula M. Allaf,[1] Iris V. Rivero,[2] Ilia N. Ivanov[3]

[1]Department of Industrial Engineering, German-Jordanian University, Amman 11180, Jordan
[2]Department of Industrial and Manufacturing Systems Engineering, Iowa State University, Ames 50011, Iowa
[3]Center for Nanophase Materials Sciences, Oak Ridge National Laboratory, Oak Ridge 37831, Tennessee
Correspondence to: I. V. Rivero (E-mail: rivero@iastate.edu)

ABSTRACT: The apparent inability of a single biomaterial to meet all the requirements for tissue engineering scaffolds has led to continual research in novel engineered biomaterials. One method to provide new materials and fine-tune their properties is via mixing materials. In this study, a biodegradable powder blend of poly(ε-caprolactone) (PCL), polyglycolide (PGA), and poly(ethylene oxide) (PEO) was prepared and three-dimensional interconnected porous PCL/PGA scaffolds were fabricated by combining cryomilling and compression molding/polymer leaching techniques. The resultant porous scaffolds exhibited co-continuous morphologies with ~50% porosity. Mean pore sizes of 24 and 56 μm were achieved by varying milling time. The scaffolds displayed high mechanical properties and water uptake, in addition to a remarkably fast degradation rate. The results demonstrate the potential of this fabrication approach to obtain PCL/PGA blend scaffolds with interconnected porosity. In general, these results provide significant insight into an approach that will lead to the development of new composites and blends in scaffold manufacturing. © 2015 Wiley Periodicals, Inc. J. Appl. Polym. Sci. **2015**, *132*, 42471.

KEYWORDS: biodegradable; blends; porous materials; properties and characterization; synthesis and processing

Received 28 November 2014; accepted 5 May 2015
DOI: 10.1002/app.42471

INTRODUCTION

Tissue engineering is an encouraging therapeutic strategy that aims to fabricate biological tissue for the replacement of diseased and/or damaged tissues or organs, also capable to overcome drawbacks of artificial organs and organ transplantation.[1,2] Typically cells isolated from a patient and supplemented with growth factors are cultured in a three-dimensional (3D) porous scaffold to regenerate new tissues.[1,3] With this ultimate goal, the scaffold must exhibit a combination of physical and chemical properties suited for the particular application, in addition to basic requirements for tissue engineering. In general, the scaffold should be biocompatible and bioresorbable with a 3D interconnected porous structure, and mechanical properties closely matching those of the target tissue. Also, the scaffold degradation rate should match the tissue healing rate allowing proper tissue regeneration.[4–8] Several synthetic polymers—such as poly(ε-caprolactone) (PCL), polyglycolide (PGA), and polylactide (PLA)—as well as natural polymers—such as collagen, alginate, and chitosan—have been investigated as suitable scaffold matrices.[4–6] However, the inability of a neat biocompatible polymer to fulfill all the demands for tissue engineering scaffolds has led to increased interest in blends and composites amid advantages of more improved and tunable properties (degradation, biocompatibility, thermal, barrier, and mechanical), improved integration with native tissue, and lower cost.[9,10] Polymer blends offer a simple approach to combine the properties of materials without the added complexity of development of a new copolymer.[11–13] Blending polymers with different degradation profiles may allow customization of the physical and mechanical properties along with the rate of degradation.[11–13]

Among the scaffold fabrication technologies, the selective polymer extraction from co-continuous immiscible blends is one of the promising technologies, enabling control over scaffold morphology.[14–16] Scaffolds with open interconnected porosity and different pore size distributions can be designed by this technique.[15–18] In 2011, we reported the development of another novel phase separation/porogen extraction approach based on cryomilling combined with compression molding and selective polymer leaching techniques (CCM-SPL) to prepare co-continuous porous scaffolds. The underlying mechanism behind the CCM-SPL technique is the formation of homogeneous blends from immiscible polymer pairs during cryomilling followed by phase separation and coarsening of the resulting co-continuous blend morphologies during hot molding. The last

step of the CCM-SPL approach is selective leaching of one continuous polymer phase, which produces interconnected porosity in the scaffold. The approach was demonstrated with the preparation of co-continuous PCL scaffolds utilizing poly(ethylene oxide) (PEO) as a water-soluble porogen.[19] Details on the effects of several process parameters on scaffold properties were reported earlier.[19,20] The main advantages of the approach are its simplicity, interconnected porosity, and cylindrical wall structures that are strong enough for load-bearing tissue regeneration applications.[19,20] The CCM-SPL processing technique can be applied to a large variety of polymer blends and composites, enabling high level of control over pore size and porosity while minimizing the presence of potentially harmful solvents.

This study demonstrates the preparation of PCL/PGA scaffolds from PCL/PGA/PEO blends using the CCM-SPL approach and utilizing the PEO water-soluble porogen. PCL is a semicrystalline, biocompatible but hydrophobic material with low cell affinity that has been advocated to be particularly appropriate for long-term implantable devices because of its low degradation rate (>2 years).[12,21,22] PGA is a highly crystalline aliphatic polyester which exhibits a high tensile modulus and very low solubility in organic solvents.[22,23] It is more hydrophilic than PCL and degrades significantly faster by hydrolysis (3–4 months), losing mechanical integrity in aqueous solution or in vivo between 2 and 4 weeks, posing challenges for long-term applications.[13,22–26] Consequently, it is expected that a PCL/PGA blend could offer wide possibilities to optimize degradation, mechanical properties, and hydrophilicity, while improving bioactivity, in addition to overcoming inherent limitations of its constituents.[12,13] Aghdam *et al.* (2012) reported electrospinning nanofibrous blends of PCL and PGA with higher hydrophilicity as well as mechanical properties as the PGA content was increased.[12] The molecular characteristics of the polymers, the blending ratio,[12,13] as well as the processing conditions should enable tunability of the PCL/PGA blend performance to meet the strict application requirements.

However, aliphatic polyesters are mutually immiscible,[27] and thus, form multiphase structures. Properties of multiphase materials are generally affected by three main factors, namely, the properties of the component polymers, the adhesion between the phases, and the blend morphology.[18] Therefore, compatibilization is needed to make blends with fine microstructures and good mechanical properties. In the CCM-SPL technique, the solid-state cryomilling is used to homogeneously blend and compatibilize the polymeric components.[28–31] By using polymers with significantly different melting temperatures, PGA can be retained in the form of as-milled particles at a processing temperature below its melting point, while PCL and PEO melt forming the co-continuous matrix of the blend. The initially homogeneous dispersion of PGA is predicted to be sustained during the hot molding step due to low bulk flow, lack of shear forces during the compression molding process, and stronger interfaces between the milled components. The resulting melt-molded polymer blend will have well-dispersed PGA particles in a PCL/PEO matrix. In this study, PCL, PGA, and PEO were mixed in a 40 : 10 : 50 wt % composition ratio. A small amount of PGA (20 : 80 wt % PGA : PCL) was used as a filler; this amount should affect the properties of scaffolds[12] while not inhibiting the continuity of the PCL matrix. Cryomilled polymer mixtures were compression-molded and PEO was removed by immersing the scaffolds in water. The produced scaffolds were tested for hydrophilicity, morphological, thermal, mechanical, and degradation properties demonstrating the potential of this fabrication approach as a route to obtain porous PCL/PGA blend scaffolds with interconnected porosity, higher hydrophilicity, and degradability. The work presented in this article was later extended by Jonnalagadda *et al.* (2014, 2015) to establish and validate the proper cryomilling time that would yield to optimal chondrocyte adhesion, proliferation, and GAG secretion for articular cartilage tissue engineering.[32,33]

EXPERIMENTAL

Materials

Poly(ε-caprolactone) (CAPA6506) powder (only 2% above 600 μm), with a number average molecular weight (M_n) of ~47,500 was obtained from Perstorp UK Limited, UK. It has a melting temperature range of 58–60°C and a density of 1.14 g/cm^3 (at 60°C). Poly(glycolide) in an extruded-pellet form was purchased from Lakeshore Biomaterials/Brookwood Pharmaceuticals, Inc., USA. It has a specific gravity of 1.53, a glass transition temperature (T_g) of 39.9°C (DSC), a melting point (T_m) of 221.9°C (DSC), and a crystallinity of 35.4% (DSC). Poly(ethylene oxide) fine powder (Mesh-20, 96–100%) with a viscosity average molecular weight (M_v) of 100,000 was purchased from Sigma-Aldrich, USA. It has a density of 1.13 g/cm^3 (at 25°C), a T_g of −67°C, and a T_m of 65°C. Although PCL, PEO, and PGA are FDA approved for biomedical use, nonmedical polymer grades were used in this study since no cell-culture studies were planned at this stage. PCL and PEO polymers were selected in accordance with our previous studies, which established the success of the CCM-SPL approach in producing porous PCL from the selected PEO porogen[19,20]; furthermore, other research groups also demonstrated successful fabrication using the melt-mixing approach.[14,16] Distilled water was used in porogen extraction. Phosphate-buffered saline (PBS) (Sigma-Aldrich, USA) and silica gel (Sigma-Aldrich, USA) were also used in the study. A 0.01 M PBS (0.138 M NaCl; 0.0027 M KCl) solution was obtained by dissolving one pouch of PBS powder in 1 L of distilled water.

Scaffold Fabrication

Prior to polymer blending, PGA pellets (1.5 g) were ground into powder by cryogenically milling in a SPEX 6770 Sample-Prep Freezer mill (SPEX CertiPrep Group, Inc., USA). Actual milling was performed for 18 min to attain PGA powders with a particle size comparable to those of as-received PCL and PEO (Figure 1). Next, PCL/PGA scaffolds were fabricated via the previously described CCM-SPL approach.[19,20] In brief, manually mixed 1.5 g powder samples of 40 : 10 : 50 wt % PCL/PGA/PEO were first dried in 15 mL glass vials in a vacuum desiccator (Scienceware, Sigma-Aldrich, USA) with silica gel desiccant for at least 48 h prior to milling. Next, samples were blended in the SPEX 6770 Freezer mill and then dried in the desiccator for at least 48 h before molding. Subsequently, large flakes were manually removed and samples were loaded in a mold with

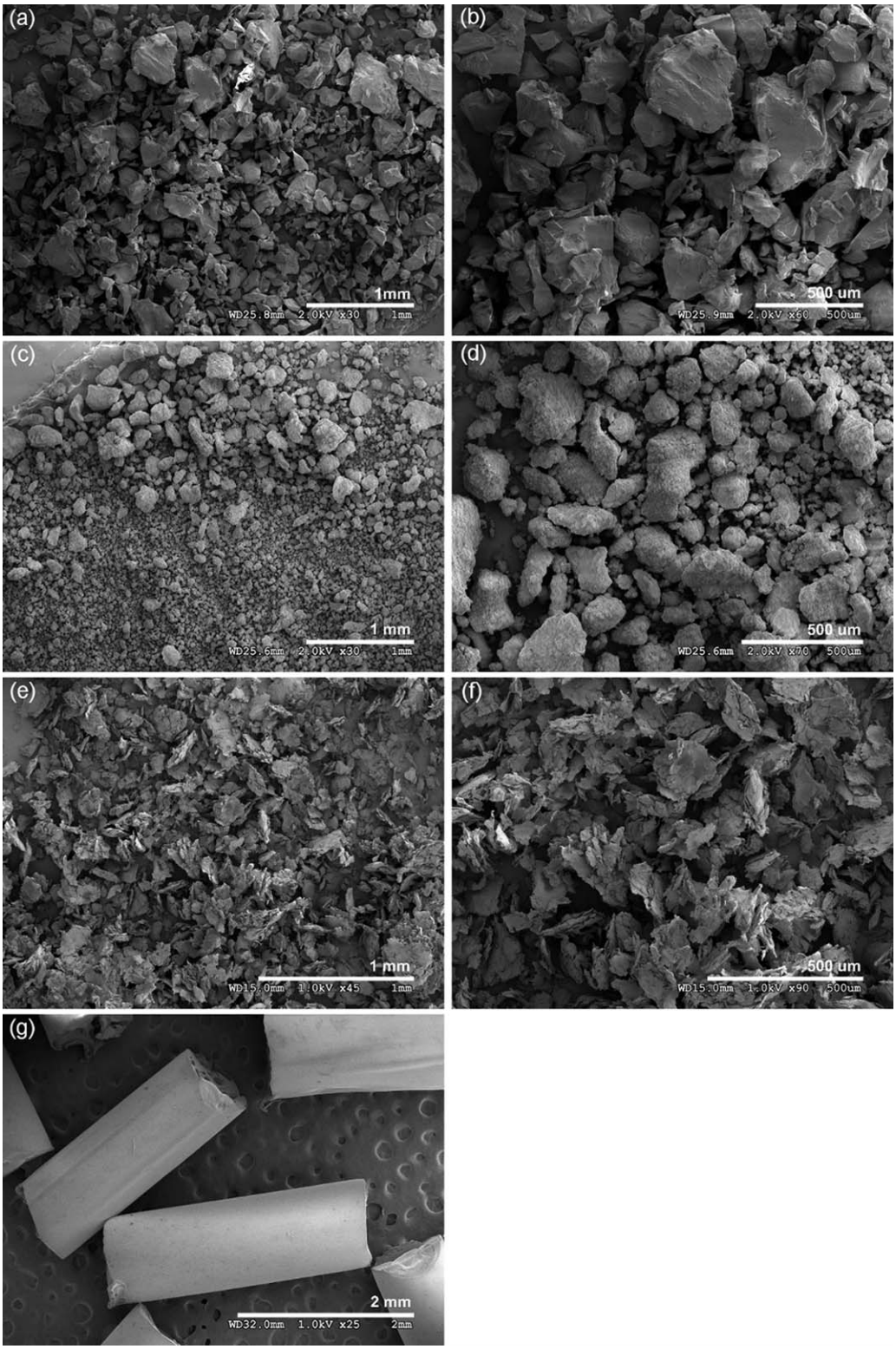

Figure 1. SEM micrographs of as-received (a,b) PCL and (c,d) PEO; (e,f) ground PGA; and (g) as-received PGA.

~9-mm-diameter cylindrical cavities. Assuming homogeneous blend compositions and using materials densities, the mass loadings were calculated to slightly overfill the mold cavities to maintain a constant volume of ~827.0 mm^3 for each sample upon full closure of the mold. Then samples were compression molded at 100°C into ~9 mm × 13 mm cylinders in a Carver bench top laboratory press (Carver, Inc., Wabash, IN, USA). The fabricated product characteristics are sensitive to the major

process parameters such as cryomilling time, molding temperature, and blend composition.[19,20] In this study, the effect of cryomilling time on scaffold properties was investigated through milling powders at two milling times: 36 (PCL/PGA36) and 90 (PCL/PGA90) min of actual milling time; times were selected for comparison with neat PCL results.[20]

After molding, samples were immersed in distilled water in their 15 mL glass vials, at room temperature, and the water was changed every day until the wet sample achieved constant weight (~10 days) in order to dissolve the water-soluble PEO porogen. After porogen extraction, the samples were removed from water, blotted dry, and dried in a vacuum oven at ~40°C until the dry sample achieved constant weight (~5 days). At last, scaffolds were stored in the desiccator until characterization. Samples were weighed and measured after the molding, porogen leaching, and drying steps. Each sample's diameter and height were repeatedly measured with an electronic caliper ($n = 5$); measurements were then averaged for volume calculation. PCL scaffolds were also fabricated from PCL/PEO 50 : 50 wt % using the same approach to serve as a control sample.

Scaffold Characterization

Cross-sectional morphologies of the scaffolds were observed under a Hitachi S-4300 SE/N high-resolution field emission scanning electron microscope (FESEM, Hitachi, Japan) after sputter coating with a gold/palladium alloy in a Technics Hummer V Sputter Coater. Samples were fractured in liquid nitrogen and mounted on the SEM sample holder using an aluminum stub with double-sided carbon tape. Two cross-sections were observed on each sample to investigate homogeneity throughout the depth of the scaffold. Image analysis was carried out using SIMAGIS software (Smart Imaging Technologies, Houston, TX, USA) in order to obtain quantitative information on pore size. The porosity of the scaffold samples was determined via a gravimetric method using the apparent density of the scaffold (ρ_{scaffold}) estimated by means of dividing its mass by its volume, and the bulk density of the nonporous scaffold material ($\rho_{\text{PCL+PGA}}$):[16]

$$\text{Porosity}\ (\%) = \left(1 - \frac{\rho_{\text{scaffold}}}{\rho_{\text{PCL+PGA}}}\right) \times 100\% \quad (1)$$

Related to porosity is the extent of continuity of the porogen phase, which was evaluated using the weight of the PEO porogen in the sample before and after extraction, both calculated from the weight fraction of PEO in the blend assuming homogeneous blends:[16,17]

$$\%\text{Continuity of PEO} = \frac{\text{weight PEO}_{\text{initial}} - \text{weight PEO}_{\text{final}}}{\text{weight PEO}_{\text{initial}}} \times 100\% \quad (2)$$

The water uptake (bulk water absorption) was evaluated according to eq. (3) using the wet weight (m_{wet}) of the samples after complete porogen leaching and the dry weight (m_{dry}) after drying in the vacuum oven. Then the fraction of scaffold volume filled with water was calculated via dividing the volume of pores occupied with water by the total wet volume of the scaffold, where the volume of pores occupied by water was deduced from the weight difference between the dry and wet samples:[34,35]

$$\text{Water uptake}\ (\%) = \left(\frac{m_{\text{wet}} - m_{\text{dry}}}{m_{\text{dry}}}\right) \times 100\% \quad (3)$$

The compressive properties of scaffold samples were determined using a Shimadzu AGSJ Series Autograph universal testing machine (Shimadzu Manufacturing Co., Ltd., Osaka, Japan) at room temperature using a cross-head speed of 1 mm/min. The elastic compressive modulus and compression strength of the sample were determined utilizing calculated stress–strain (σ–ε) curves, where the modulus was determined via linear regression analysis as the slope of the initial linear elastic portion of the σ–ε curve and the compressive strength was measured at ~10% strain in the plateau region,[36,37] after toe region correction for the zero-strain point following the ASTM D695-08 standard methodology.[38]

Thermal degradation studies were carried out on PCL/PGA36 scaffolds to assess if polymers degraded during fabrication by thermogravimetric analysis (TGA) on a TA Instruments Q5000IR thermogravimetric analyzer (TA Instruments, USA). Specimens (~5–15 mg) were heated in platinum pans from 25 to 1000°C under inert flowing nitrogen (50 mL/min) at a heating rate of 10°C/min. OriginPro 8.5 software (OriginLab Corporation, Northampton, MA, USA) was used to analyze the thermogravimetric (TG) and derivative thermogravimetric (DTG) curves for residual mass and peak degradation temperature (T_d), respectively. Differential scanning calorimetry (DSC) experiments were conducted to provide information about the thermal properties, crystalline structure, and compatibility of the blend scaffolds after fabrication, particularly since crystallinity plays an important role in the physical properties and the biodegradability of the scaffolds.[39] DSC specimens (~5–10 mg) were analyzed in a TA Instruments Q1000 differential scanning calorimeter (TA Instruments, USA) using aluminum pans and nitrogen purge gas (50 mL/min). Specimens were first quenched at −10°C/min to −100°C before being heated to 260°C at a heating rate of 10°C/min. They were then maintained at 260°C for 1 min and subsequently cooled to −100°C at a cooling rate of 10°C/min. After holding at −100°C for 1 min, specimens were finally heated to 260°C at 10°C/min. The resulting DSC curves were analyzed using OriginPro 8.5 software to determine transition temperatures and enthalpies. The melting and crystallization temperatures (T_m and T_c) were noted as temperatures corresponding to the peaks of melting and crystallization, respectively. The glass transition temperature (T_g) was noted as the temperature corresponding to the midpoint of the glass transition. The melting (ΔH_m) and crystallization (ΔH_c) enthalpies were calculated from corresponding peak areas below and above the baseline, respectively. The degree of crystallinity of a polymer (X_c) was determined by the fusion enthalpy method using eq. (4),[17,40] with the value of $\Delta H_{m,\ \text{PCL},\ 100\%\text{crystal}}$ (the melting enthalpy of 100% crystalline PCL) = 139.5 J/g,[34] and $\Delta H_{m,\ \text{PGA},\ 100\%\ \text{crystal}}$ (the melting enthalpy of 100% crystalline PGA) = 183.2 J/g:[41]

$$X_{c,A}\ (\%) = \frac{\Delta H_{m,A}}{\Delta H_{m,A,100\%\ \text{crystal}}} \times \frac{1}{\left(\frac{wt_A\%}{100}\right)} 100\% \quad (4)$$

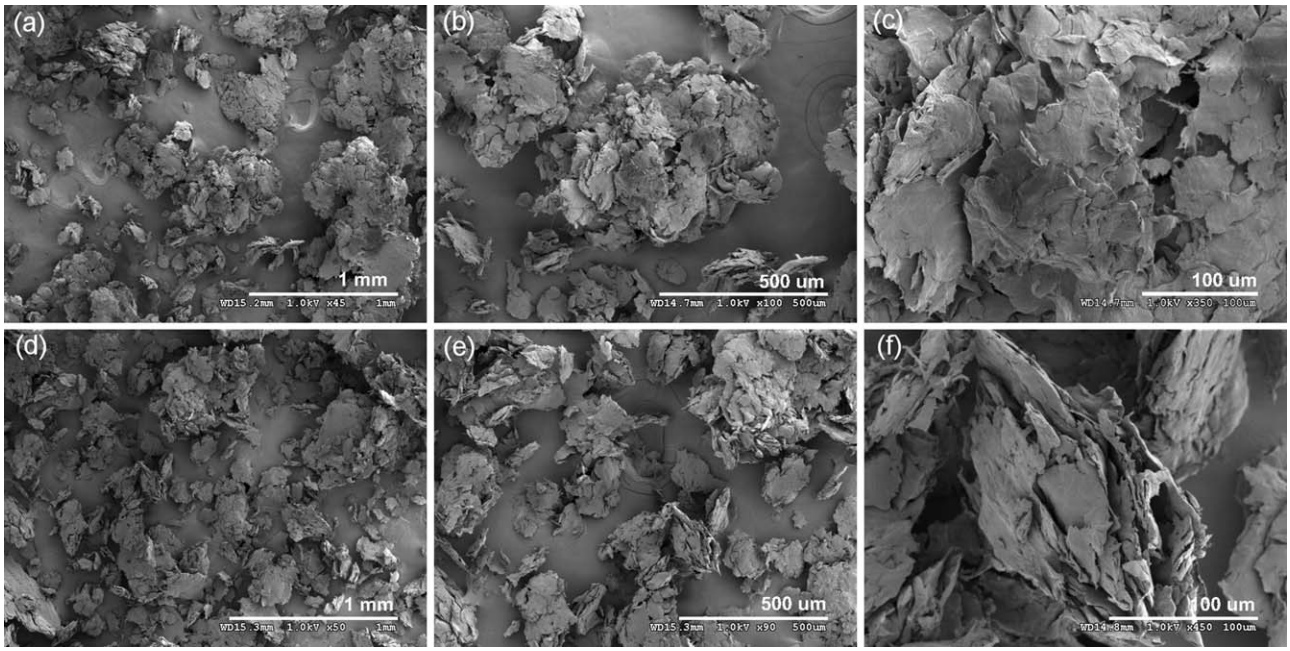

Figure 2. SEM micrographs of PCL/PGA/PEO (40 : 10 : 50) powders cryomilled for (a–c) 36 and (d–f) 90 min. Three magnifications are shown.

where $\Delta H_{m,A}$ and $wt_A\%$ designate the measured melting enthalpy and weight percentage of polymer A in the scaffold, respectively. First heating scans were analyzed to reflect both the type of existing materials and the general physical structure (amorphous, crystalline, and semicrystalline) developed during processing. Second heating scans correspond to materials properties after erasing their thermal histories.

Scaffold *In Vitro* Degradation Study

Hydrolytic *in vitro* degradation of porous PCL/PGA36 scaffolds was performed in PBS solution over a 5-week period in an incubator (Percival Scientific, Inc., Boone, IA, USA) at 37°C under static conditions. Nine pre-weighed dry samples (~9 × 13 mm) were immersed in glass vials containing ~15 mL of PBS solution (pH 7.6) and stored in the incubator. The PBS solution was changed every 2 days (pH dropped from 7.6 to a minimum of 6.6). Samples were removed after 1, 3, and 5 weeks for degradation analysis. At each point of time, three samples were analyzed and the obtained values were averaged. Samples were washed with distilled water and vacuum dried at ~40°C for 3 days to assure dryness and no thermal degradation. Mass loss and compression properties in unconfined compression were analyzed. Mass loss was calculated by comparing the initial weight (m_0) with the weight measured at a given point of time (m_t) as follows:

$$\text{Mass loss } (\%) = \frac{m_0 - m_t}{m_0} \times 100\% \quad (5)$$

Statistical Analysis

All quantitative results were expressed as mean ± standard deviation. Measurements were obtained from at least triplicate samples. Analysis of variance (ANOVA) was used to test for statistical differences among different scaffolds mean properties using OriginPro 8.5 software. The Tukey test was used to compare each two means. Data were taken to be significant when a p-value of 0.05 or less was obtained.

RESULTS AND DISCUSSION

PCL/PGA/PEO Cryomilled Powder Blends

PGA pellets with approximate mean dimensions of 515 × 1515 μm [Figure 1(g)] were cryomilled to produce a powder on a similar size scale as the PCL and PEO powders. SEM micrographs of a PGA powder cryomilled for 18 min are shown in Figure 1(e,f). Cryomilled PGA particles exhibited a flake-like morphology with particle size ranging from ~35 to ~540 μm, whereas unmilled PCL particles appeared angular with smooth surfaces and particle size ranging from ~40 to ~685 μm [Figure 1(a,b)]. Moreover, unmilled PEO particles had aggregate, rough shapes with particle sizes ranging from ~8 to ~400 μm [Figure 1(c,d)]. Although the three particle morphologies were different, the size scales were comparable.

SEM micrographs of PCL/PGA/PEO powders cryomilled for 36 and 90 min are shown in Figure 2(a–c and d–f), respectively. Flake-like individual and layered particles were apparent in the micrographs. The layered appearance resulted from layers of material which were fractured, flattened, and then cold-welded during the cryomilling process. Particles were irregular with particle sizes in the range of ~65 to ~1175 μm and ~60 to ~1490 μm, respectively. However, individual PCL, PGA, and PEO phase domains or layers are not differentiable from SEM images. Because of the limitations of microscopy, effect of cryomilling time on phase domains will be discerned from the size of pores and pore walls after extracting the PEO.

PCL/PGA36 Scaffolds

Figure 3(a–c) shows a typical morphology of the PCL/PGA36 scaffolds prepared from PCL/PGA/PEO powders cryomilled for

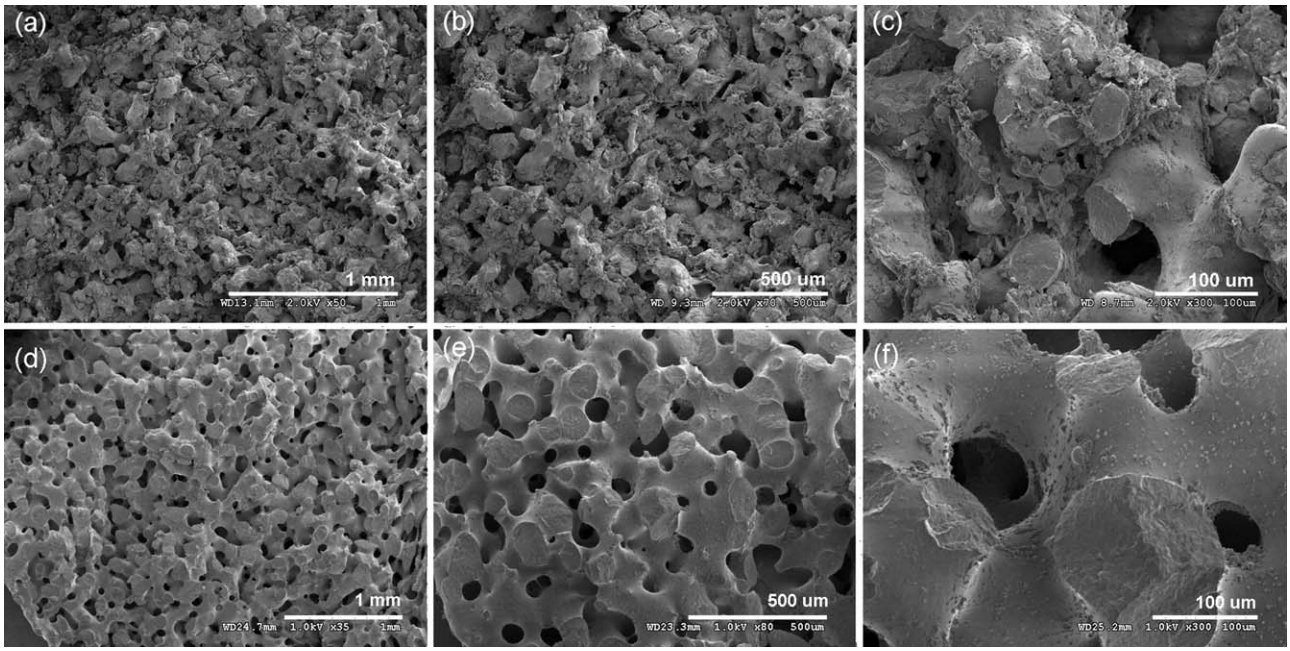

Figure 3. SEM micrographs of scaffolds molded at 100°C and made from (a–c) PCL/PGA/PEO (40 : 10 : 50) powders and (d–f) PCL/PEO (50 : 50) powders cryomilled for 36 min. Three magnifications are shown.

36 min. It can be seen that the scaffolds were porous, which is confirmed by the gravimetric results (Table I). The high-magnification micrograph provided in Figure 3(c) reveals several interesting features of the scaffolds. First, the structure is characterized by two co-continuous networks of cylindrical pores and cylindrical walls exhibiting a smooth texture; however, the pore network contains inclusions. These inclusions are most likely PGA inclusions, which were entrapped in the PEO phase and settled down on the cylindrical walls upon PEO extraction. These inclusions will, most likely, affect cell penetration into the scaffold and the scaffold's compressive strength. Furthermore, they will affect scaffold degradation behavior, especially during the early stages, when PGA degrades fast and probably catalyzes the degradation of the scaffold.

The pore size distribution appeared unimodal with a mean pore size estimated at ~56 μm, which is within the optimum pore sizes for cell ingrowth, 20–60 μm[17]; but less than that reported optimal for tissue regeneration, 100 and 500 μm.[1,17] However, pore size may be increased by lowering cryomilling time and/or increasing molding temperature.[19,20] Furthermore, pore sizes were smaller than those obtained from the PCL36 control scaffolds prepared at the same cryomilling time, with mean pore size estimated at ~80 μm [Figure 3(d–f)]. This may be attributed to the PGA filler confinement effect, which may slow or hinder coarsening of the polymer phases.

Calculated porosities and levels of continuity for the scaffolds are reported in Table I. Porosity values are lower than the theoretically predicted ones (Table I). The reason behind this

Table I. Characteristics of PCL/PGA Scaffolds and Control Samples Milled for Two Different Cryomilling Times: 36 and 90 Min and Molded at 100°C

Scaffold designation	PCL/PGA36	PCL/PGA90	PCL36	PCL90
Mean pore size (μm)	56 ± 10	24 ± 2	80 ± 4	36 ± 5
Porosity (%)	49.56 ± 0.33	48.62 ± 0.33	49.11 ± 0.41	46.67 ± 1.98
Continuity of PEO (%)	101.12 ± 0.59	98.39 ± 0.19	99.45 ± 0.69	97.40 ± 0.10
Theoretical porosity[a] (%)	55.3	55.3	50.2	50.2
Water uptake (%)	81.45 ± 1.36	85.60 ± 2.76	64.63 ± 4.45	86.05 ± 2.36
Volume occupied with water (%)	47.77 ± 0.73	50.30 ± 1.43	35.67 ± 2.54	48.23 ± 1.39
Volumetric change$_{w-d}$ (%)	−0.86 ± 0.61	−2.49 ± 0.72	−5.12 ± 0.43	−9.59 ± 0.62
Compressive modulus (MPa)	25.51 ± 1.06	23.47 ± 4.35	59.07 ± 0.48	83.69 ± 3.36
Compressive strength $\sigma_{\varepsilon=0.1}$ (MPa)	1.15 ± 0.05	1.77 ± 0.11	3.07 ± 0.02	4.11 ± 0.03

[a] Theoretical porosity was estimated from the volume fraction of porogen in the scaffold, assuming that 50% of PGA was lost with leached PEO; volume of scaffold was calculated from volumes of its constituents (PGA, PEO, and PCL); masses of constituents were estimated from their respective percentages of the measured mass of the scaffold before leaching PEO.

discrepancy is that theoretical porosity has been calculated gravimetrically assuming homogeneous mixing of all polymers, and thus extraction of all PEO porogen and 50% of the PGA. However, as previously mentioned, PGA particles are deposited in the scaffolds reducing accessible porosity.

These results thus confirm the co-continuous structure, since the part remaining after dissolution of the porogen is self-supporting and has a mass approximately equal to that in the original blend; in other measures, porosity is approximately equal to the volume fraction of the porogen(s) and the porogen phase is almost 100% continuous, i.e., interconnected. The results demonstrate the feasibility of creating interconnected porous scaffolds from blends using the CCM-SPL approach. They illustrate that the incorporation of the PGA filler does not inhibit the formation of a co-continuous morphology. They further reveal the high degree of mixing obtained by cryogenic milling. However, filler residue may block some of the pores if it remains in the scaffold after porogen extraction.

Table I further reports water uptake, percentage of scaffold wet volume occupied by water, and percentage change in scaffold volume. The water uptake is high; scaffolds were filled to ~82% of the weight of the porous scaffolds by water. In other words, about 96% of the scaffold's wet porosity was filled by water. It should be mentioned here that some of the scaffold void volume was filled by the PGA inclusions decreasing the amount of space available for water uptake. These results illustrate that most of the scaffolds' internal porosity is accessible to aqueous solutions. Comparing these scaffolds to the PCL control scaffolds with ~65% water uptake reveals a ~26% increase in water uptake with the same milling time. However, Aghdam *et al.* reported a 78% increase in water uptake of 84% porosity electrospun PCL/PGA(80/20) blend nanofibrous scaffolds.[12] Nonetheless, this increase cannot be only attributed to the PGA, since the PCL/PGA36 scaffolds had smaller pores, which may have caused the increase in water uptake. Furthermore, the addition of hydrophilic PEO can significantly enhance the wetting ability of the scaffolds.[8,42] The water uptake (bulk water absorption) of scaffolds is a good indicator of their bulk hydrophilicity.[43] Hydrophilicity supports cell culture and growth, nutrients infiltration into the porous scaffolds, and homogeneous tissue regeneration.[44,45] Therefore, the hydrophilicity of the fabricated PCL/PGA scaffolds is significant. Oh *et al.* listed some approaches used to improve hydrophilicity of biodegradable polymer scaffolds; these include: (i) coating with some hydrophilic polymers or cell-adhesive proteins and (ii) blending with hydrophilic polymers such as dextran and PEO derivatives.[44] PEO is known to be compatible with PCL,[46] thus PEO residue may have strongly bonded to the PCL matrix. In addition, the high cryomilling forces may induce covalent chain scission, and subsequent chemical coupling of the blend components, often termed *in situ* compatibilization.[28] Thus, the probable bonding or grafting of PEO onto PCL may have contributed to the higher scaffold hydrophilicity. It should be mentioned here that several scaffold properties such as degradation, wet mechanical properties, and drug release kinetics are correlated to the wetting and water uptake characteristics.

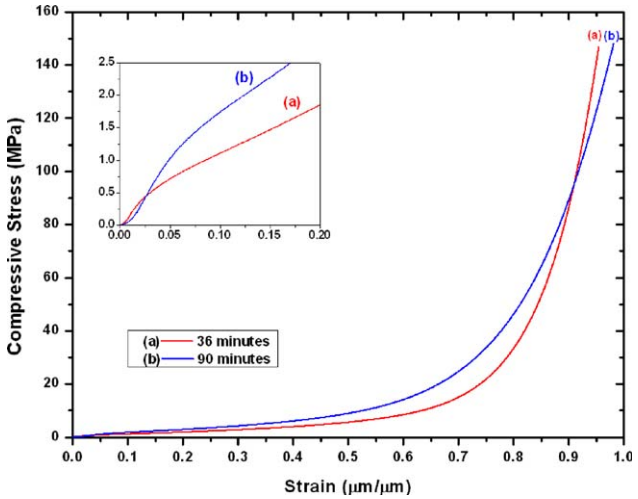

Figure 4. Compression stress–strain curves for (a) PCL/PGA36 and (b) PCL/PGA90 porous scaffolds. Inset figure shows a magnification of small strain data. [Color figure can be viewed in the online issue, which is available at wileyonlinelibrary.com.]

Compression tests were carried out on the porous scaffolds to investigate their compressive properties. An essential condition for tissue engineering scaffolds is to match the mechanical properties of the healthy tissue until the regenerated tissue takes over that particular function.[4,6,16] None of the scaffolds failed during testing; all tests were terminated when reaching 90% of the capacity of the compression testing machine. The results of the compression tests were interpreted in terms of σ–ε curves. Figure 4 shows a typical σ–ε curve for the investigated PCL/PGA36 scaffolds and the compressive properties derived from the curves are summarized in Table I. These curves—which consist of four zones: toe, linear elastic, plateau, and densification—show typical behavior of porous polymeric foams under compression.[37,47,48] The co-continuous cylindrical scaffold morphology imparts high stiffness and strength due to the thick interconnected cylindrical walls; with compressive modulus values of 25.51 ± 1.06 MPa, the scaffolds' modulus is in the range reported for human load-bearing tissue.[49,50] However, the compressive properties of these scaffolds are significantly lower than those for the PCL36 control scaffolds fabricated at the same cryomilling time, which exhibited compressive moduli of ~59 MPa, and compressive strengths at 10% strain of ~3.1 MPa. These results may be attributed to the smaller cylindrical wall size which we earlier ascribed to the PGA filler confinement effect, and/or to low adhesion between the PCL and PGA phases, which should be unlikely with cryomilling, since the process has been advocated to create stronger interfaces due to physical entanglements and/or chemical bonding combined with the massive amount of interfaces created by the milling process.[28–31] Furthermore, the PCL/PGA36 scaffolds occasionally showed large porosities extending to the scaffolds surfaces, which may be attributed to either trapped air bubbles or directional shrinkage during molding, and may have also caused reduction and variability in the compressive properties. Still, the compressive properties are better compared to scaffolds with thin pore walls such as the PCL scaffolds fabricated with salt

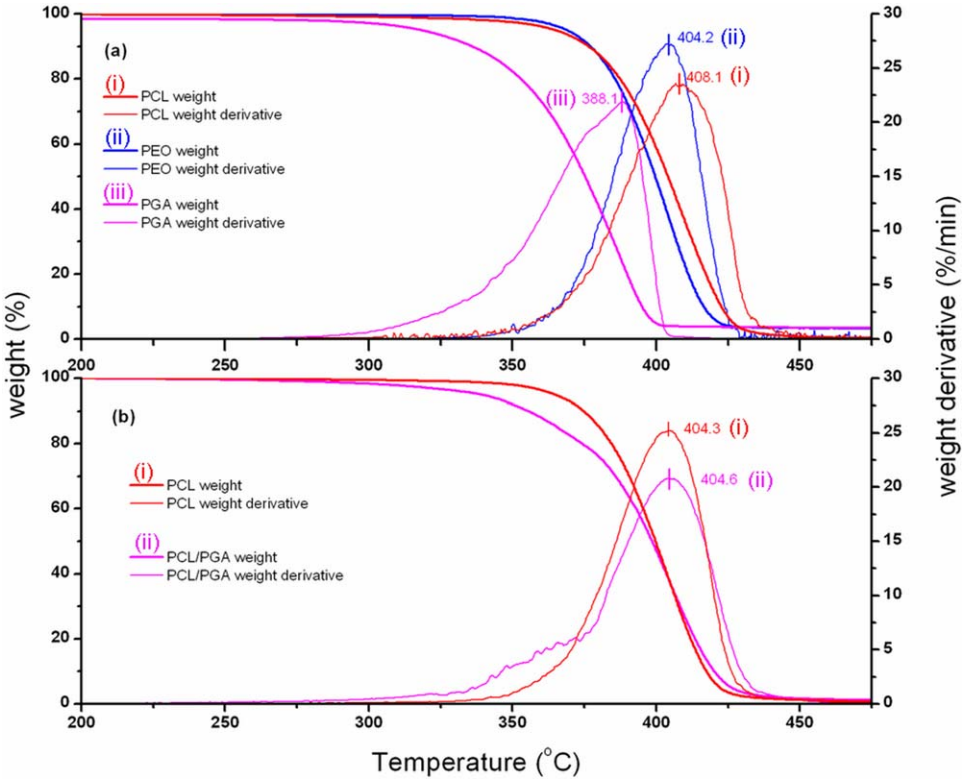

Figure 5. Thermogravimetric curves (TG and DTG) for (a) pure powder components and (b) scaffolds cryomilled for 36 min. [Color figure can be viewed in the online issue, which is available at wileyonlinelibrary.com.]

particulates,[19] or dual salt/polyethylene glycol (PEG) porogens.[42]

Thermal degradation of PCL/PGA36 scaffolds and as-received pure powder components was investigated with TGA in a nitrogen atmosphere at a heating rate of 10°C/min. Figure 5 shows the thermogravimetric (TG) and derivative thermogravimetric (DTG) curves for the pure powder components and the scaffolds. The peak degradation temperatures (T_d) of the PCL, PGA, and PEO pure powders were 408, 388, and 404°C, respectively. PGA curve shows weight loss starting at ~280°C, assuring that the polymer did not decompose during the DSC investigations. Residual masses reveal the presence of minor amounts of impurities or polymer carbonization for the PGA and PEO polymers. Scaffolds' TG curves show the superimposed effect of the PGA component addition on the PCL curve, with an earlier and accelerated startup of degradation upon the incorporation of the PGA. Similarly, the residual mass showed a minor increase. Finally, the T_d of the PCL (404°C) did not change significantly, suggesting no significant degradation due to the fabrication process.

The DSC thermal analysis was conducted between −100°C and 260°C in three scans—first heating, cooling, and second heating—to enable the collection of information about the existing component materials as well as the physical structure developed during processing due to the thermal and mechanical histories. The DSC thermograms for the heating and cooling scans are shown in Figure 6. The heating scans show, in increasing order of temperature, the glass transition of PCL, the endothermic melting peak of PCL crystallites overlapping with the glass transition of PGA, and finally, the endothermic melting peak of PGA crystallites. On the other hand, the cooling scans show, in decreasing order of temperature, the exothermic melt crystallization peak of PGA crystallites, the exothermic melt crystallization peak of PCL crystallites overlapping with the glass transition of PGA, and finally, the glass transition of PCL. Tables II and III summarize the main information derived from

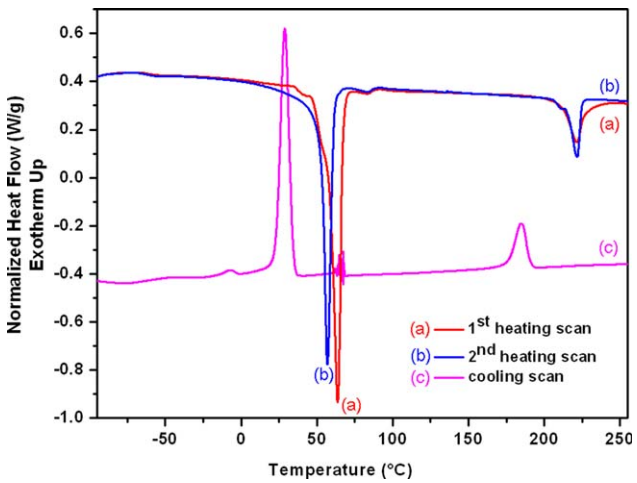

Figure 6. DSC (a) first heating, (b) second heating and (c) cooling scans for PCL/PGA36 scaffold samples recorded at 10°C/min. [Color figure can be viewed in the online issue, which is available at wileyonlinelibrary.com.]

Table II. DSC Melting Data for PCL-Based Scaffold Samples

	PCL				PGA		
Scaffold designation	T_g (°C)	T_m (°C)	ΔH_m (J/g)	X_c (%)	T_m (°C)	ΔH_m (J/g)	X_c (%)
First heating scan							
PCL/PGA36	−61	64	−71	64	222	−13.6	37
PCL36	−62	64	−87	63			
Nonporous PCL36	−62	64	−84	60			
Second heating scan							
PCL/PGA36	−62	58	−61	55	222	−12.0	33
PCL36	−63	57	−77	55			
Nonporous PCL36	−62	57	−75	53			

the DSC heating and cooling curves, respectively, for the PCL/PGA36 scaffolds as well as PCL36 control scaffolds and nonporous PCL36 scaffolds for comparison purposes. Some differences can be seen between the first and second heating curves, which correspond to materials properties after fabrication and after erasing their thermal histories, respectively. These differences will be discussed in the following paragraphs.

T_g was estimated at the midpoint of the segment of the inflectional tangent between the extrapolated onset and endpoint temperatures. The T_g of the amorphous part of PCL appears at about −62°C for all scaffolds in all DSC scans (Table II). The melting peaks of PCL in the first scan appear at higher peak temperatures (by ~6°C) than in the second scan; this may be accredited to slower cooling rates during fabrication and, thus, to the presence of larger, more perfect crystals.[51] The melting peaks in the first scan consist of multiple peaks (Figure 6) which is attributed to multimodal crystal size distribution,[52] with small size, less perfect crystals melting at lower temperatures and/or crystal reorganization (crystal perfection) during melting.[52] Other experiments such as higher heating rate DSC scans are necessary to provide more insight into the origin of these peaks.[52,53] On the other hand, the melting peaks in the second scan only show low-temperature tails (Figure 6), which is ascribed to dispersion of crystal sizes.[52] It is worth noting that T_m did not vary significantly, when compared to pure PCL. Moreover, the crystallinities of PCL calculated from the first scan are higher by ~8% than those obtained from the second scan (Table II), which is also attributed to the slower cooling rates during fabrication. It should be mentioned, however, that accurate determination of the enthalpies was difficult to achieve due to difficulty in establishing a baseline for the integration, especially with the overlapping PGA glass transition for PGA-containing scaffolds. A straight-line baseline was used for all peak integrations. DSC data for nonporous PCL36 scaffolds that were made by cryomilling powders to 36 min follow the same trends as the porous blend scaffolds, except for slightly lower PCL crystallinities (Tables II and III).

Table III. DSC Crystallization Data for PCL-Based Scaffold Samples

	PCL			PGA	
Cooling scan	T_g (°C)	T_c (°C)	ΔH_c (J/g)	T_c (°C)	ΔH_c (J/g)
PCL/PGA36	−62	29	52	185	12.5
PCL36	−61	30	64		
Nonporous PCL36	−61	31	64		

The melting peak of PGA appears at ~222°C in both heating scans (Figure 6 and Table II). This is explained by the fact that scaffolds were molded at 100°C, thus, below the melting and crystallization temperatures of PGA (Tables II and III). The crystallinity of PGA calculated from the first scan is higher (by ~5%) than that obtained from the second scan (Table II); this is attributed to some crystallization occurring above the PGA glass transition during the slow cooling of the molded scaffolds (supplier reported T_m and X_c are 221.9°C and 35.4%, respectively). The DSC results, thus, do not indicate any discernible compatibilization effects between the PCL and PGA polymers.[13] However, the results demonstrate that the fabricated PCL/PGA36 scaffolds are highly crystalline ($X_{c,PCL} = 64\%$; $X_{c,PGA} = 37\%$), showing higher melting temperatures and crystallinities after fabrication (first scan) than after cooling from melt (second scan). High crystallinity levels, in addition to pore wall cylindrical structure, contribute to the high mechanical strength of the scaffold. However, low PCL/PGA interfacial adhesion negatively contributes to strength. Similar trends have been reported for PCL, PLLA, and PCL/PLLA porous membranes fabricated by a freeze-extraction method.[53]

Effect of Cryomilling Time

The effect of cryomilling time on scaffold pore morphology and physical properties was investigated by milling PCL/PGA/PEO powders for 90 min and then molding at 100°C. Figure 7(a–c) shows the morphology of the scaffolds; mean pore size estimated from the SEM images is 24 μm and the pore size distribution was apparently unimodal. Thus, it is evident that pore size decreases with increasing cryomilling time, which may be attributed to a physical reduction in the scale of mixing with increasing time. Same trends were obtained for PCL90 porous scaffolds, which showed a decrease in mean pore size to 36 μm [Figure 7(d–f)]. The calculated porosity values (Table I) for the PCL/PGA90 scaffolds are slightly lower than those for the PCL/PGA36 scaffolds. This is also attributed to the physical reduction in the scale of mixing with increasing cryomilling time

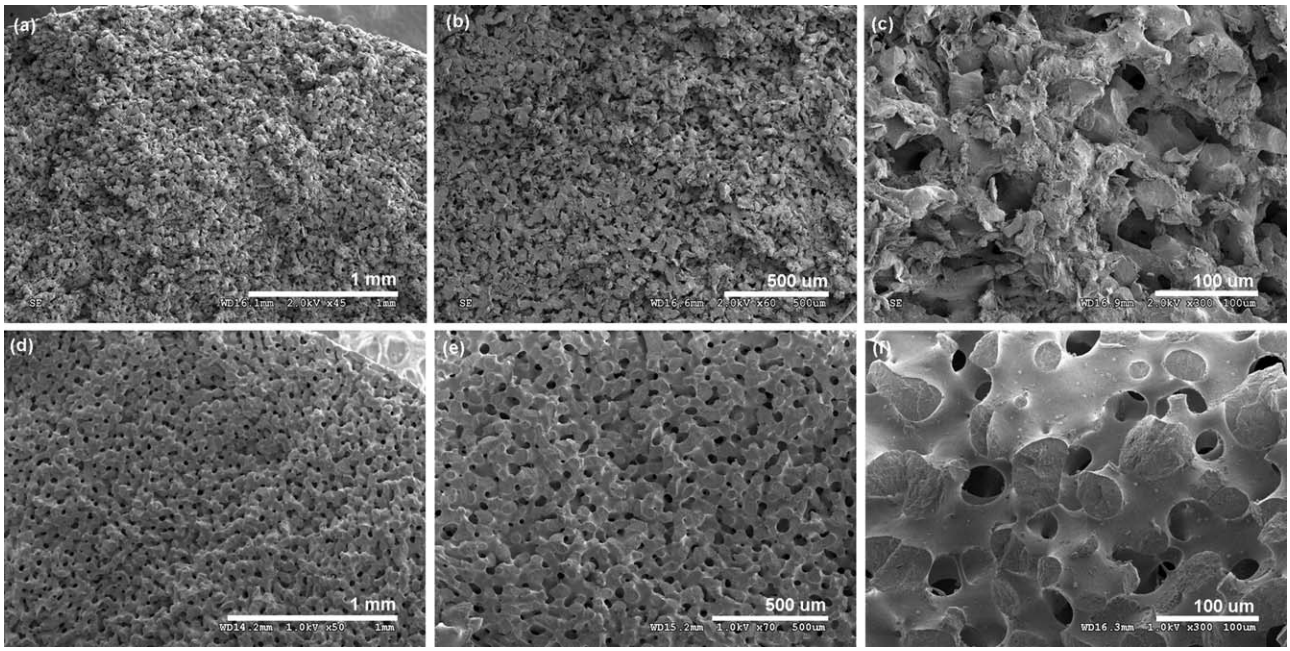

Figure 7. SEM micrographs of (a–c) PCL/PGA90 and (d–f) PCL90 scaffolds molded at 100°C. Three magnifications are shown.

and, thus, higher amounts of PEO and PGA trapped in the scaffolds. The water uptake was high; scaffolds were filled to ~86% of the weight of the porous scaffolds by water, i.e., about 100% of the scaffolds' wet porosity was filled by water. The difference from scaffolds cryomilled at 36 min, though small, is statistically significant and may be attributed to small volumetric differences and the increase in capillary pressure and water holding capacity as pore size decreases. The compressive modulus means (Table I) of these PCL/PGA90 scaffolds were not significantly different from PCL/PGA36 due to large variability in the values exhibited by the scaffolds cryomilled for 90 min. Compressive strength (Table I), however, increased significantly with increased time, corresponding to the smaller mean pore size. These results imply that cryomilling time is an important factor to control pore size as well as mechanical properties of final scaffold.

Degradation Study

Hydrolytic *in vitro* degradation of the porous PCL/PGA36 scaffolds was performed in a PBS solution over a 5-week period in an incubator at 37°C under static conditions. The outcome of the degradation in terms of mass loss and change of compressive properties as a function of degradation time is reported in Table IV and graphically shown in Figure 8. Furthermore, σ–ε curves for the degraded samples over time are shown in Figure 9. The weight of the dried samples slowly decreased reaching ~90.5% of its initial value after 5 weeks of degradation. However, the samples did not show any apparent surface erosion or fragmentation during degradation. Referring to the extremely slow degradation rate of PCL and very fast rate of PGA,[21–26] this weight loss may be accredited to the fast degradation of the small PGA deposits, which should account for approximately 10% of the scaffolds weight, again assuming homogeneous mixing of the polymers. This loss reassures the nature of the deposits and suggests an easy and effective way for removing PGA residue from the internal pores of the scaffolds.

Analysis of the compression tests results revealed that the strength of the samples slowly decreased reaching ~76.5% of its initial value after 5 weeks of degradation. Strength is correlated with mass loss, since these deposits squeeze in the pores increasing the resistance to the compressive force. The compressive modulus, however, showed a marked decrease during the first week down to ~45.3% of its initial value, then progressively decreased to ~35% of its initial value after 5 weeks of degradation. Similar results were reported by Schindler *et al.* (2013) for an electrospun 3 : 1 PCL/PGA–copolymer blend, with a marked decrease during the first week followed by a progressive increase in the following 5 weeks.[13] These results may be attributed to the interplay between several factors in the pore walls, such as

Table IV. Mass and Mechanical Properties During *In Vitro* Degradation of PCL/PGA36 Scaffolds

	Week 0	Week 1	Week 3	Week 5
Mass loss (%)	-	0.80 ± 0.11	5.14 ± 0.40	9.43 ± 0.15
Compressive modulus (MPa)	25.51 ± 1.06	11.56 ± 1.36	9.65 ± 0.92	8.94 ± 0.36
Compressive strength $\sigma_{\varepsilon=0.1}$ (MPa)	1.15 ± 0.05	1.09 ± 0.05	0.92 ± 0.05	0.88 ± 0.08

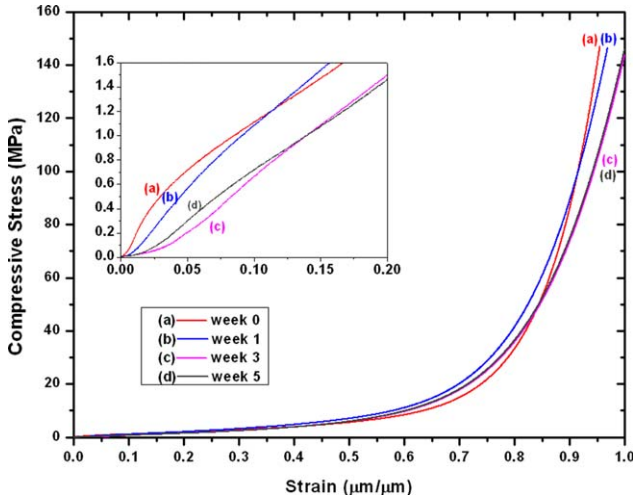

Figure 8. Mass, compressive modulus and compressive strength variation with time during *in vitro* degradation of PCL/PGA36 porous scaffolds. [Color figure can be viewed in the online issue, which is available at wileyonlinelibrary.com.]

reduction in PGA molecular weight, PGA mass loss, and changes in crystallinity during incubation, as well as the presence of large air voids in some scaffolds. The results are consistent with PGA reported behavior, where mechanical integrity in aqueous solution is lost between 2 and 4 weeks,[25,26] which also suggests that the addition of PCL prolonged the degradation of the blend to more than 5 weeks.

In a comparable study, Lam *et al.* investigated the *in vitro* degradation of 70% porous PCL scaffolds (6.5 × 6.5 × 13.5 mm^3) prepared from ~1.7 mm filaments via a fused deposition modeling (FDM) extruder in PBS (10 mL) at 37°C for up to 6 months.[53] They reported no differences in scaffold morphology with an average mass loss of 0.72% at 6 months; while an increase in compressive stiffness and yield strength (tested at 1 mm/min) from 2.4 to 3.6 MPa and 0.7 to 1.0 MPa, respectively, was attributed to increased crystallinity during incubation. The results of our study illustrate the ability to manipulate the PCL degradation through incorporation of PGA in a porous structure. The scaffolds maintained their mechanical integrity and high compressive properties after 5 weeks of degradation, which represent an appropriate period of time for tissue culture and degradation studies, suggesting their suitability in load-bearing tissue engineering applications.

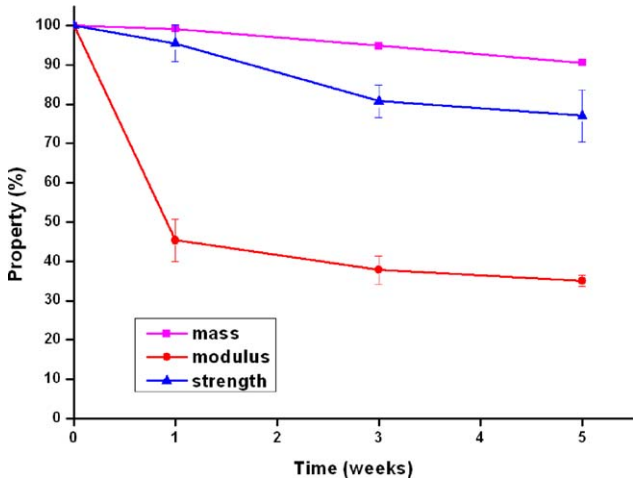

Figure 9. Compression stress–strain curves for *in vitro* degraded PCL/PGA36 porous scaffolds at week (a) 0, (b) 1, (c) 3, and (d) 5. Inset figure shows a magnification of small strain data. [Color figure can be viewed in the online issue, which is available at wileyonlinelibrary.com.]

CONCLUSIONS

This study demonstrated the feasibility of producing interconnected porous PCL/PGA scaffolds with two networks of interconnected cylindrical pores and pore walls using the CCM-SPL approach allowing to blend otherwise immiscible components. Addition of PGA resulted in interconnected ~50% porous scaffolds with a similar morphology to the PCL scaffolds fabricated under the same processing conditions, except for the smaller mean pore sizes (24 and 56 μm) and the presence of appreciable amounts of inclusions filling the pores, which may be removed via leaching the PEO under dynamic conditions to drive these smaller inclusions out of the scaffold. Other PCL/PGA scaffolds properties include higher hydrophilicity and good compressive mechanical properties. Furthermore, those blend scaffolds had an appreciably fast degradation compared to degradation of PCL scaffolds reported in the literature and PCL polymer slow degradation rates.[53–55] The CCM-SPL processing of blended scaffold is a promising approach for design of novel systems with tunable properties for tissue engineering. Future work will concentrate on studies to increase pore size and eliminate deposits.

ACKNOWLEDGMENTS

The authors gratefully acknowledge the Texas Tech University Imaging Center, Department of Biological Sciences, for use of the Hitachi S-4300SE/N (NSF MRI 04–511). Thermal analysis was performed under project CNMS2009-052 at the Center for Nanophase Materials Sciences, which is a DOE Office of Science User Facility.

REFERENCES

1. Ikada, Y. *J. Roy. Soc. Interface* **2006**, *3*, 589.
2. Wu, S.; Liu, X.; Yeung, K. W.; Liu, C.; Yang, X. *Mat. Sci. Eng. R* **2014**, *80*, 1.
3. Lu, H.; Hoshiba, T.; Kawazoe, N.; Chen, G. *Biomaterials* **2011**, *32*(10), 2489.
4. Chung, C.; Burdick, J. A. *Adv. Drug Deliver. Rev.* **2008**, *60*, 243.
5. Vial, X.; Andreopoulos, F. M. *Curr. Rheumatol. Rev.* **2009**, *5*, 51.
6. Puppi, D.; Chiellini, F.; Piras, A. M.; Chiellini, E. *Prog. Polym. Sci.* **2010**, *35*(4), 403.
7. Liu, Y.; Lim, J.; Teoh, S. H. *Biotechnol. Adv.* **2013**, *31*(5), 688.

8. Chen, B. Y.; Wang, Y. S.; Mi, H. Y.; Yu, P.; Kuang, T. R.; Peng, X. F.; Wen, J. S. *J. Appl. Polym. Sci.* **2014**. DOI: 10.1002/A41181.
9. Vertuccio, L.; Gorrasi, G.; Sorrentino, A.; Vittoria, V. *Carbohyd. Polym.* **2009**, *75*, 172.
10. Gabay, O.; Sanchez, C.; Taboas, J. M. *Joint Bone Spine* **2010**, *77*(4), 283.
11. Bramfeldt, H.; Sarazin, P.; Vermette, P. *Polym. Degrad. Stab.* **2008**, *93*, 877.
12. Aghdam, R. M.; Najarian, S.; Shakhesi, S.; Khanlari, S.; Shaabani, K.; Sharifi, S. *J. Appl. Polym. Sci.* **2012**, *124*(1), 123.
13. Schindler, C.; Williams, B. L.; Patel, H. N.; Thomas, V.; Dean, D. R. *Polymer* **2013**, *54*, 6824.
14. Washburn, N. R.; Simon, C. G.; Tona, A.; Elgendy, H. M.; Karim, A.; Amis, E. J. *J. Biomed. Mater. Res.* **2002**, *60*(1), 20.
15. Sarazin, P.; Favis, B. D. *Biomacromolecules* **2003**, *4*, 1669.
16. Reignier, J.; Huneault, M. A. *Polymer* **2006**, *47*, 4703.
17. Sarazin, P.; Roy, X.; Favis, B. D. *Biomaterials* **2004**, *25*, 5965.
18. Pötschke, P.; Paul, D. R. *Polym. Rev.* **2003**, *43*(1), 87.
19. Allaf, R. M.; Rivero, I. V. *J. Mater. Sci. Mater. M.* **2011**, *22*, 1843.
20. Allaf, R. M.; Rivero, I. V.; Abidi, N.; Ivanov, I. N. *J. Biomed. Mater. Res. B* **2013**, *101*(6), 1050.
21. Chiono, V.; Vozzi, G.; D'Acunto, M.; Brinzi, S.; Domenici, C.; Vozzi, F.; Ahluwalia, A.; Barbani, N.; Giusti, P.; Ciardelli, G. *Mater. Sci. Eng. C* **2009**, *29*, 2174.
22. Doppalapudi, S.; Jain, A.; Khan, W.; Domb, A. *J. Polym. Adv. Technol.* **2014**, *25*(5), 427.
23. Nair, L. S.; Laurencin, C. T. *Prog. Polym. Sci.* **2007**, *32*, 762.
24. Ishaug-Riley, S. L.; Okun, L. E.; Prado, G.; Applegate, M. A.; Ratcliffe, A. *Biomaterials* **1999**, *20*, 2245.
25. Tan, L.; Yu, X.; Wan, P.; Yang, K. *J. Mater. Sci. Technol.* **2013**, *29*(6), 503.
26. Okamoto, M.; John, B. *Prog. Polym. Sci.* **2013**, *38*, 1487.
27. Eastmond, G. C. In Advances in Polymer Science: Biomedical Applications/Polymer Blends; Springer Berlin-Heidelberg: New York, **2000**, vol. *149*, 59.
28. Stranz, M.; Köster, U.; Katzenberg, F. *J. Metastab. Nanocryst. Mater.* **2005**, *24*, 609.
29. Zhu, Y. G.; Li, Z. Q.; Zhang, D.; Tanimoto, T. *J. Appl. Polym. Sci.* **2006**, *99*(2), 501.
30. Zhu, Y. G.; Li, Z. Q.; Zhang, D.; Tanimoto, T. *J. Polym. Sci. B* **2006**, *44*(8), 1161.
31. Vertuccio, L.; Gorrasi, G.; Sorrentino, A.; Vittoria, V. *Carbohyd. Polym.* **2009**, *75*(1), 172.
32. Jonnalagadda, J.; Rivero, I. V.; *J. Mech. Behav. Biomed. Mater.* **2014**, *40*, 33.
33. Jonnalagadda, J. B.; Rivero, I. V.; Dertien, J. S. *J. Biomat. Sci.-Polym. Ed.* **2015**, *26*(7), 401.
34. Lebourg, M.; Serra, R. S.; Estellés, J. M.; Sánchez, F. H.; Ribelles, J. G.; Antón, J. S. *J. Mater. Sci. Mater. M.* **2008**, *19*(5), 2047.
35. Ghosh, S.; Viana, J. C.; Reis, R. L.; Mano, J. F. *J. Mater. Sci. Mater. M.* **2007**, *18*, 185.
36. Sarazin, P.; Virgilio, N.; Favis, B. D. *J. Appl. Polym. Sci.* **2006**, *100*(2), 1039.
37. Bureau, M. N. In Thermoplastic Foam Processing: Principles and Development; Gendron, R., Ed.; CRC Press: Boca Raton, **2005**, 235.
38. Test Method for Compressive Properties of Rigid Plastics, ASTM Standard D 695-08, **2008**.
39. Andrady, A. L. In Physical Properties of Polymers Handbook; Mark, J. E., Ed.; Springer: New York, **2007**, 951.
40. Zhao, J.; Yuan, X.; Cui, Y.; Ge, Q.; Yao, K. *J. Appl. Polym. Sci.* **2004**, *91*(3), 1676.
41. Standard Specification for Poly(glycolide) and Poly(glycolide-co-lactide) Resins for Surgical Implants with Mole Fractions Greater Than or Equal to 70% Glycolide, ASTM Standard F 2313-08, **2008**.
42. Thadavirul, N.; Pavasant, P.; Supaphol, P. *J. Biomed. Mater. Res. A* **2013**, DOI: 10.1002/jbm.a.35010.
43. Wan, Y.; Chen, W.; Yang, J.; Bei, J.; Wang, S. *Biomaterials* **2003**, *24*(13), 2195.
44. Oh, S. H.; Kang, S. G.; Kim, E. S.; Cho, S. H.; Lee, J. H. *Biomaterials* **2003**, *24*(22), 4011.
45. Lee, C. T.; Huang, C. P.; Lee, Y. D. *Biomacromolecules* **2006**, *7*, 2200.
46. Maglio, G.; Malinconico, M.; Migliozzi, A.; Groeninckx, G. *Macromol. Chem. Physic.* **2004**, *205*(7), 946.
47. Correlo, V. M.; Boesel, L. F.; Pinho, E.; Costa-Pinto, A. R.; Alves da Silva, M. L.; Bhattacharya, M.; Mano, J. F.; Neves, N. M.; Reis, R. L. *J. Biomed. Mater. Res. A* **2009**, *91*(2), 489.
48. Mills, N. J. Polymer Foams Handbook: Engineering and Biomechanics Applications and Design Guide; Elsevier-Butterworth-Heinemann: Burlington, **2007**.
49. Varga, F.; Drzik, M.; Handl, M.; Chlpik, J.; Kos, P.; Filová, E.; Rampichova, M.; Necas, A.; Trc, T.; Amler, E. *Physiol. Res.* **2007**, *56*(Suppl 1), S61.
50. Sabir, M. I.; Xu, X.; Li, L. J. *Mater. Sci.* **2009**, *44*, 5713.
51. Menczel, J. D.; Judovits, L.; Prime, R. B.; Bair, H. E.; Reading, M.; Swier, S. In Thermal analysis of polymers: fundamentals and applications; Menczel, J. D.; Prime, R. B., Eds.; John Wiley & Sons: Hoboken, New Jersey, **2009**, 7.
52. Lebourg, M.; Anton, J. S.; Gomez Ribelles, J. L. *Eur. Polym. J.* **2008**, *44*, 2207.
53. Lam, C. X.; Hutmacher, D. W.; Schantz, J. T.; Woodruff, M. A.; Teoh, S. H. *J. Biomed. Mater. Res. A* **2009**, *90*(3), 906.
54. Middleton, J. C.; Tipton, A. *J. Biomaterials* **2000**, *21*, 2335.
55. Brown, M.; Farrar, D. *Plast. Rubber Compos.* **2008**, *37*(2–4), 46.